Biomedicine & Pharmacotherapy 171 (2024) 116119

Contents lists available at ScienceDirect

Biomedicine & Pharmacotherapy

journal homepage: www.elsevier.com/locate/biopha

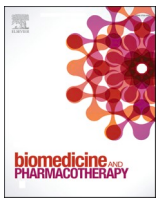

Cardioprotection by the adiponectin receptor agonist ALY688 in a preclinical mouse model of heart failure with reduced ejection fraction (HFrEF)

Sungji Cho [a], Keith Dadson [a], Hye Kyoung Sung [a], Oyeronke Ayansola [a], Ali Mirzaesmaeili [b], Nina Noskovicova [c], Yimu Zhao [d,e], Krisco Cheung [f], Milica Radisic [d,e,f], Boris Hinz [c,g], Ali A. Abdul Sater [b], Henry H. Hsu [h], Gary D. Lopaschuk [i], Gary Sweeney [a,*]

[a] Department of Biology, York University, Toronto, ON, Canada
[b] School of Kinesiology and Health Science, York University, Toronto, ON, Canada
[c] Faculty of Dentistry, University of Toronto, Toronto, ON M5S3E2, Canada
[d] Toronto General Hospital Research Institute, Toronto, ON M5G 2C4, Canada
[e] Institute of Biomaterials and Biomedical Engineering, University of Toronto, Toronto, ON M5S 3G9, Canada
[f] Department of Chemical Engineering and Applied Chemistry; University of Toronto, Toronto, ON M5S 3E5, Canada
[g] Laboratory of Tissue Repair and Regeneration, Keenan Research Centre for Biomedical Science, St. Michael's Hospital, Toronto, ON M5B 1T8, Canada
[h] Allysta Pharmaceuticals Inc. Bellevue, WA, USA
[i] Department of Pediatrics, University of Alberta, Edmonton, AB, Canada

ARTICLE INFO

Keywords:
Adiponectin
Heart failure
Therapeutic
Fibrosis
Inflammation
Metabolism

ABSTRACT

Aims: Adiponectin has been shown to mediate cardioprotective effects and levels are typically reduced in patients with cardiometabolic disease. Hence, there has been intense interest in developing adiponectin-based therapeutics. The aim of this translational research study was to examine the functional significance of targeting adiponectin signaling with the adiponectin receptor agonist ALY688 in a mouse model of heart failure with reduced ejection fraction (HFrEF), and the mechanisms of cardiac remodeling leading to cardioprotection.

Methods and results: Wild-type mice were subjected to transverse aortic constriction (TAC) to induce left ventricular pressure overload (PO), or sham surgery, with or without daily subcutaneous ALY688-SR administration. Temporal analysis of cardiac function was conducted via weekly echocardiography for 5 weeks and we observed that ALY688 attenuated the PO-induced dysfunction. ALY688 also reduced cardiac hypertrophic remodeling, assessed via LV mass, heart weight to body weight ratio, cardiomyocyte cross sectional area, ANP and BNP levels. ALY688 also attenuated PO-induced changes in myosin light and heavy chain expression. Collagen content and myofibroblast profile indicated that fibrosis was attenuated by ALY688 with TIMP1 and scleraxis/periostin identified as potential mechanistic contributors. ALY688 reduced PO-induced elevation in circulating cytokines including IL-5, IL-13 and IL-17, and the chemoattractants MCP-1, MIP-1β, MIP-1alpha and MIP-3α. Assessment of myocardial transcript levels indicated that ALY688 suppressed PO-induced elevations in IL-6, TLR-4 and IL-1β, collectively indicating anti-inflammatory effects. Targeted metabolomic profiling indicated that ALY688 increased fatty acid mobilization and oxidation, increased betaine and putrescine plus decreased sphingomyelin and lysophospholipids, a profile indicative of improved insulin sensitivity.

Conclusion: These results indicate that the adiponectin mimetic peptide ALY688 reduced PO-induced fibrosis, hypertrophy, inflammation and metabolic dysfunction and represents a promising therapeutic approach for treating HFrEF in a clinical setting.

* Correspondence to: Department of Biology, York University, Toronto, M3J 1P3 ON, Canada.
E-mail address: gsweeney@yorku.ca (G. Sweeney).

https://doi.org/10.1016/j.biopha.2023.116119
Received 29 October 2023; Received in revised form 28 December 2023; Accepted 29 December 2023
Available online 4 January 2024

1. Introduction

Heart failure (HF) is a leading cause of mortality worldwide [1] and a primary cause is PO-induced cardiac remodeling, characterized by cardiomyocyte left ventricular hypertrophy (LVH), myocardial fibrosis, inflammation and metabolic alterations [2–4]. Cardiac remodeling occurs as an adaptive response to pathological stress; however, persistent stress leads to adverse remodeling in the myocardium and development of HF [5]. In the presence of chronic hypertension a pathological hypertrophy can develop, which is characterized by an excessive increase in ventricular dimensions, accompanied by myocardial dysfunction and fibrosis [2–4]. A number of studies have shown that modulating hypertrophic growth of the myocardium can actually afford clinical benefit without provoking hemodynamic compromise. Despite extensive attempts to develop effective pharmacological interventions, there remains an unmet need for patients with HF [6,7]. Hence, developing novel therapeutic approaches is necessary.

Defective adiponectin action due to reduced circulating or interstitial adiponectin levels or cellular adiponectin resistance has been implicated in the pathophysiology of HF [8]. Correlative clinical studies have identified low levels of adiponectin as a risk factor for cardiometabolic diseases (CMD) with a negative correlation between circulating adiponectin levels and HF [9,10]. This suggests that improving the effectiveness of adiponectin by either raising its levels in the circulation or promoting its signaling could be used as a treatment for HF [11,12]. Adiponectin has been shown to improve metabolic effects in various organs including liver, adipose tissue, skeletal muscle and heart [13,14]. Indeed, experimental strategies to elevate adiponectin in preclinical models confer protection against various forms of HF, including PO, ischemic reperfusion injury and diabetic cardiomyopathy [15–18]. Furthermore, mimicking adiponectin action with the small molecule AdipoRon has shown beneficial effects in various HF models [15,19,20]. Notably, adverse cardiac remodeling is exacerbated in mice lacking adiponectin compared to wild-type mice, which can be prevented by administration of adiponectin or AdipoRon [15,21]. The peptide ALY688 is an adiponectin receptor agonist and has previously been shown to induce adiponectin-like metabolic effects in skeletal muscle and adipocytes [22,23] protect against liver injury [24] and suppress tumor growth [25]. However, it remains unknown whether ALY688 is cardioprotective in models of heart failure.

In this study, we investigated the effect of ALY688 administration on the cardiac functional and myocardial remodeling changes in a well-established model of HF with reduced ejection fraction (HFrEF). Cardiac function was analyzed by weekly echocardiography and hypertrophic, fibrotic, inflammatory and metabolic remodeling was assessed.

2. Methods

2.1. Animal models

Experimental animals and surgical induction of PO.

All animal experimental protocols were approved by the York University Animal Care Committee and animal facilities conformed to Canadian Council on Animal Care guidelines. All mice used in this study were wild-type male C57BL/6 strain mice (10–12 wk old at time of study commencement, 0d in Fig. 1A) from Charles River Laboratories. The mice were allowed to acclimatize to the York University Vivaria environment for a minimum of 2 wk before commencement of the study. Experimental animals were housed in a temperature-controlled environment under 12 h light and 12 h dark conditions, with free access to food (a standard rodent chow diet, Lab Diet 5015) and water. All mice were then randomized into one of 3 experimental groups: Sham group – vehicle (sterile 0.9% saline) injection and sham surgery; TAC group - vehicle injection and minimally invasive transverse aortic banding (TAC) surgery; and TAC with ALY688 (TAC-A) group - ALY688 3 mg/kg injection and TAC surgery. Daily Vehicle or ALY688 treatment via subcutaneous injection began 2 d before mice were subjected to the surgery. Mice continued to receive daily subcutaneous injection for the duration of the study.

Under general anesthesia (i.p. xylazine: 0.15 mg/g; ketamine: 0.03 mg/g), hair from the chest was removed and the surgical area disinfected with betadine. A skin incision was made along the midline from the neck to the rib cage and the chest cavity was opened. The rib cage and thymus were retracted to expose the transverse aorta. A 27 g needle was used to calibrate a microclip applicator. A titanium microligation clip was applied between the origins of the innominate and left common carotid arteries, constricting the transverse aorta to the gauge of the needle. The rib cage, muscles, and skin were closed with a 6–0 USP non-absorbable silk suture. The animals were then administered with s.c. 0.03 μg/mg buprenorphine and were allowed to recover on a heating pad until fully awake. Sham surgeries were performed as above except the microligation was not applied to the transverse aorta. All mice were monitored after the procedure for normal behaviour and recovery. Cardiac function was assessed pre-surgery and then weekly by echocardiography. All mice were euthanized 5 wk post-surgery and blood was collected at this time, the heart was weighed, washed briefly in sterile PBS, and processed as required for further analysis.

2.2. Transthoracic ultrasound echocardiography

Heart function and morphology was assessed in each mouse via transthoracic echocardiographic analysis using the Vevo2100 ultrasound machine equipped with an MS400 (18–38 MHz) transducer (VisualSonics, Toronto, Canada). Assessment was done after mice were sedated in the supine position using 3% isoflurane and fur removed from the pericardial region using hair clippers and depilatory cream. Mice were then maintained in a homeostatic condition using a dorsal heating pad and very-low isoflurane (0.5 – 1%) with a target heart rate of 450–650 beats-per-minute to preserve normal contractile patterns. B-mode videos of the LV were obtained at the mid-papillary level in both parasternal short and long-axis views. M-mode recordings were taken using the parasternal short axis view at the mid-papillary level to assess LV diastolic and systolic function. Three independent views were obtained for each position, and analyses of 5–10 consecutive cardiac contractions per view were averaged using the VisualSonics platform. Standard parameters of cardiac structure and function were assessed including ejection fraction, fractional shortening, LV mass (corrected), posterior & anterior wall diameter, and internal LV diameter. Speckle-tracking based strain analysis was performed on parasternal short and long axis recordings using the VevoStrain software. Bilateral carotid blood flow velocity was assessed by Pulse-Wave Doppler measured along the left and right common carotid artery proximal to the branching of the internal carotid artery.

2.3. Cytokine analysis in circulation

Undiluted serum samples (75 μL/mouse) were processed using a bead-based multiplex immunodetection assay (Eve Technologies, Mouse Cytokine 44-Plex) for cytokines as reported in the Figures. Where a cytokine concentration was below detection threshold it was omitted from the data analysis. Serum natriuretic peptide A (ANP) was measured in 10 μL of undiluted serum by competitive Enzyme-Linked Immunosorbent Assay (Invitrogen, EIAANP).

2.4. Quantitative PCR

Gene expression in the heart was assessed in mRNA extracted from mouse heart ventricular tissue (50–100 mg/mouse). Using TRIzol Reagent (Invitrogen, Cat. 15596026), tissues were homogenized in a bead homogenizer (Fisher brand Bead Mill 24) using 4 cycles of 4 m/s for 10 s followed by 10 s rest, then digested following the TRIzol protocol. RNA concentration was determined by Varioskan Lux microplate reader

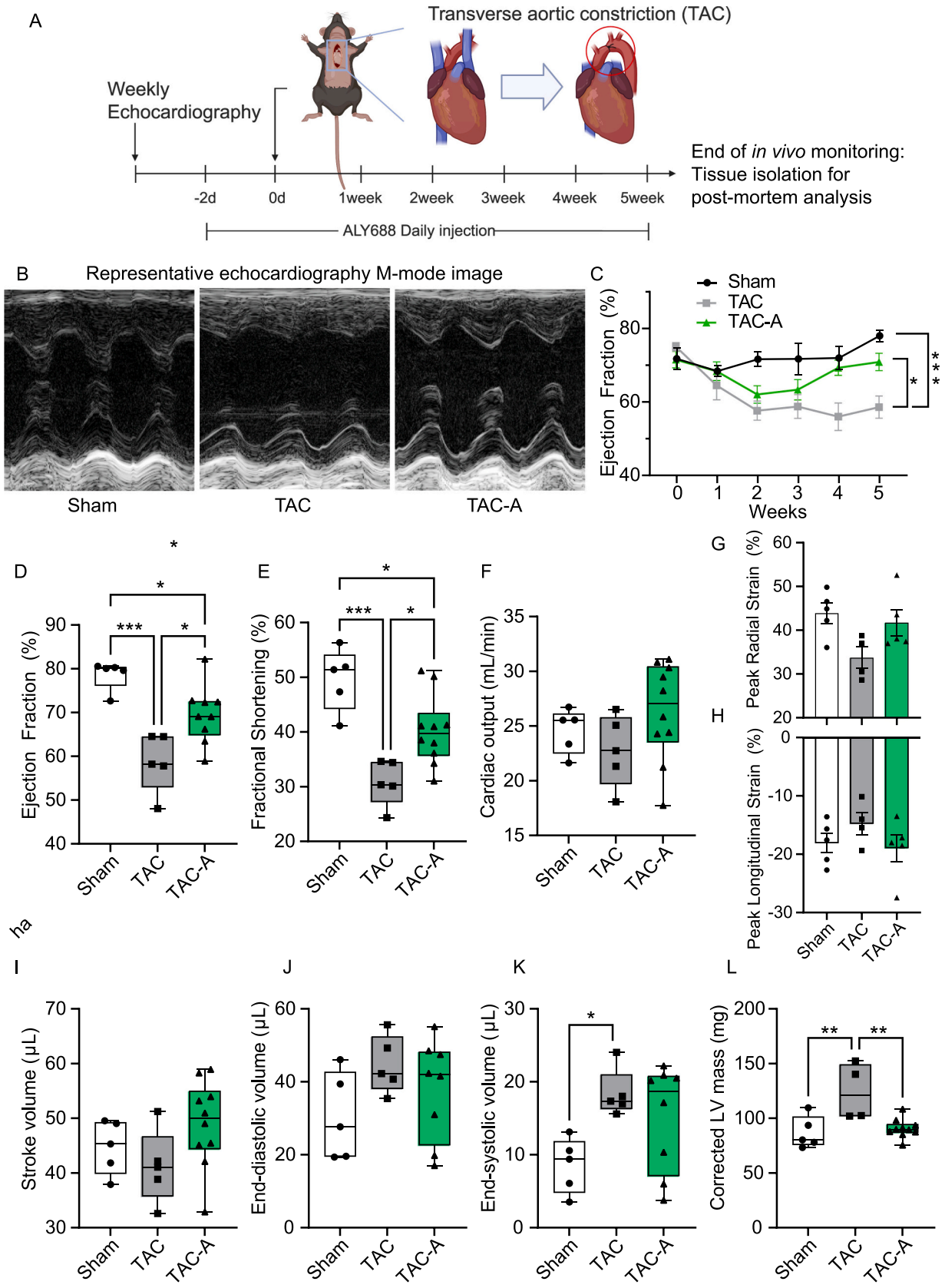

Fig. 1. ALY688 prevented systolic dysfunction caused by pressure overload. (A) Schematic overview of administration of ALY688 to male C57BL/6 mice subjected to sham or TAC surgery. Mice were administered vehicle or ALY688 3 mg/kg 2 d prior to the surgical intervention. Weekly monitoring by echocardiography to assess cardiac function and structure in mice. (B and C) (B) Representative M-mode images of echocardiography and (C) the temporal assessment of LV function by ejection fraction in each group from 0 week (baseline) to 5 wk post-surgery. (D)-(J) The parameters of cardiac function and structure at 5 weeks post-surgery were obtained by echocardiography. * = $P < 0.05$, * * = $P < 0.01$ and * ** = $P < 0.001$. n = 6–10 mice per group.

(Thermo Fisher Scientific, VL0000D0). cDNA was made from 1 μg RNA using the SuperScript IV VILO mastermix with ezDNAse enzyme following kit protocol (Thermo Fisher Scientific, Cat. 11766050). The expressions of inflammatory genes were assessed using the SsoAdvanced Universal SYBR Green Supermix (Bio-Rad Laboratories, Cat 1725274) with 1.1 μL cDNA/mouse, and the BioRad PrimePCR Inflammation Pathway Plate M384, Mmu (Bio-Rad Laboratories, Cat. 10039170). Cardiac remodeling-related genes were assessed using the TaqMan™ Fast Advanced Master Mix (Thermo Fisher Scientific, Cat 4444557) and the TaqMan™ Array (Thermo Fisher Scientific, Cat 4413259). The plates were run on a Bio-Rad CFX384 Touch Real-Time PCR Detection System (Bio-Rad Laboratories) and a QuantStudio™ Real-Time PCR system (Applied Biosystems™, Cat A28567), respectively.

2.5. Tissue processing for imaging

For histology and immunofluorescence imaging, mouse hearts were cut approximately 1–2 mm above and below the level of the papillary muscles using a sterile razor blade. Samples were then fixed in 10% neutral-buffered formalin for 24 h at 4 °C before being washed and embedded into paraffin wax. Paraffin-fixed formalin-embedded murine heart sections of 4 μm thickness were placed on glass slides, deparaffinized in xylene, and rehydrated in sequential baths of ethanol:distilled water. For immunofluorescence staining, heat-induced epitope retrieval with 0.1 M citrate buffer, pH 6 was performed and sections were further rehydrated by two washed in TBS + 0.025% TritonX-100 wash buffer. To detect myofibroblasts, primary antibodies were directed against vimentin (D21H3, rb, dilution 1:100, Cat#5741, Cell Signaling, Whitby, ON), α-smooth muscle actin (α-SMA) (1:100, α-SM1, a kind gift from Dr. Giulio Gabbiani, University of Geneva, Switzerland), and desmin as exclusion marker (1:30, Cat#M076029, Dako, Burlington, ON).[26] Isotype-specific secondary antibodies anti-rabbit IgG-TRITC (1:100, Sigma, St. Louis, Missouri, USA), Alexa647-conjugated IgG2a (1:100, Molecular Probes, Life Technologies Inc., Rockford, Illinois, USA), and anti-mouse IgG1-FITC (1:200, Southern Biotech, Birmingham, Alabama, USA) were used. Images were acquired with Zeiss Axio Observer 7 inverted confocal microscope equipped with LSM 800 scan head and ZEN software (Zeiss, Oberkochem, Germany). Cardiomyocyte cross sectional area was assessed in wheat germ agglutinin-stained sections, where n = 50 LV cardiomyocytes/mouse, 4 mice/group were measured in cross-section using Image J 1.53e (NIH, http://imagej.nih.gov/ij) calibrated to μm^2 when measured by the freehand tool. For electron microscopy, the tissue was cut into 1 mm cubes and fixed in glutaraldehyde cacodylate buffer then processed for imaging as described.[2,27] Analysis of % of α-SMA and fibrosis of Sirius red staining was performed by using Q-Path software. For scanning electron microscopy, the tissue was cut into 1 mm cubes and fixed in glutaraldehyde cacodylate buffer then processed for imaging as described.[2,27] For the differentiated human cardiac tissue staining, tissues were fixed overnight at 4 °C in 4% PFA, permeabilized, and blocked for 1 h before adding the primary antibodies as previously described.[28] Rabbit-anti-MLC2v (Abcam 79935) and mouse-anti-α-sma (Thermo Scientific 14–9760-82) were used followed by secondary antibody incubation. Goat-anti-rabbit texas red (Thermo Scientific A32795) and Goat anti-mouse (Thermo Scientific A-21240) were used as secondary antibodies. All tissues were counterstained with DAPI for the nucleus. The tissues were imaged with a Nikon R1 confocal microscope at 60x respectively.

2.6. Cardiomyocyte differentiation

BJ1D iPSCs were routinely passaged in mTesr plus media and underwent cardiomyocyte differentiation as previously described.[29] Briefly, iPSCs at 80% confluency were disassociated into single cells with Accutase (Fisher Scientific, AT104) and preplated into Matrigel-coated 12 well plates. RPMI supplemented with B27 minus insulin (Life Technologies A18956–01) and CHIR (8uM, Cayaman Chemical 131222) was added on day 0 of the differentiation. CHIR was removed after 24 hrs. WntC59 (2uM, Tocris 5148) was added on day 3 followed by removal on day 5. Cells were cultured in RPMI with B27 (Life Technologies 17504–044) on day 7 and afterward. Cardiomyocytes were disassociated after day 21. Cardiac fibroblasts (cFBs) (PromoCell CC-2904) were maintained and passaged using fibroblast growth media (Lonza CC-4526) and used before reaching passage 6.

2.7. Cardiac tissue preparation and maintenance in Biowire platform

Biowire platform was reported previously to facilitate the miniaturized cardiac tissue culture and functional evaluation using built-in force sensors and carbon electrodes [30,31]. Briefly, the array of microwell (1 mm x 5 mm x 0.3 mm) was hot embossed onto a clear polystyrene sheet. Two polymer wires (0.1 mm × 0.1 mm×9 mm) were positioned on both sides of the microwell array with glue to serve as tissue anchor points and built-in force sensors. CM and cFB were mixed at 1:1 ratio and resuspended with fibrinogen (33 mg/mL) to reach a final cell concentration of 100 million cells/mL. Thrombin (0.5uL at 25 U/mL) was added to each microwell, followed by 2uL of cell/fibrinogen suspension. Tissues were cultured in I3M (StemPro-34 complete media supplemented with 1% pen-strep, 1% GlutaMAX, 150 μg/mL transferrin and 213 ug/mL 2-phosphate ascorbic acid), with media change twice per week [31]. The seeded tissues compacted during the first week and anchored on the polymer wires at both sides of the microwell. As cardiac tissues started beating, the contractile forces generated can be calculated based on the deflection of the polymer wires under the DAPI channel. The platform with built-in force sensors can facilitate continuous non-invasive contractile functional measurements of the cardiac tissues.

2.8. Drug treatment

ALY688 treatment started on day 7 after cell seeding. 300 nM of peptide was added every two days for 2 weeks for the treated group. Control tissues do not receive drug treatment but media was replaced at the same frequency.

2.9. Tissue functional assessment

Functional assessments were performed on day 7 immediately before drug treatment and at the endpoint. Characterization of active and passive force for cardiac tissues in the Biowire II platform was performed as previously reported [30]. Briefly, tissues were placed in a sterile electrical stimulation chamber and connected with a Grass x88 stimulator. Electrical properties of the tissues, such as excitation threshold (ET) and maximum capture rate (MCR) were assessed. Recorded image sequences (paced at 1 Hz) were analyzed using a custom MATLAB code that traced the maximum deflection of the POMaC wires and calculated active force, passive tension, duration to contraction, time to peak, time from peak, contraction slope, and relaxation slope according to previously established calibration curves [30].

2.10. Metabolomics analysis

Targeted metabolomic profiles were determined in hearts isolated 5 wk post-surgery, by The Metabolomics Innovation Centre (Edmonton, AB, Canada). Heart tissue was homogenized with 3-fold dilution of 85 mL methanol and 15 mL of 10 mM phosphate buffer. Samples were then centrifuged at 14,000 rpm for 20 min and the supernatants used for LC-MS/MS analysis. A targeted quantitative metabolomics approach was used to analyze the samples using a combination of direct injection mass spectrometry (MxP500 Kit) with a reverse-phase LC-MS/MS Kit (BIOCRATES Life Sciences AG, Austria). This Kit, in combination with an ABI 5500 Q-Trap (Applied Biosystems/MDS Sciex) mass spectrometer, was used for the targeted identification and quantification of up to 630

different endogenous metabolites, including amino acids, acylcarnitines, biogenic amines, bile acids, organic acids, steroids, diacylglycerols (DGs), triacylglycerols (TGs), phosphatidylcholines, lysophosphatidylcholines, sphingomyelins, ceramides, cholesteryl esters and sugars. The method combined the derivatization and extraction of analytes, and the selective mass-spectrometric detection using multiple reaction monitoring (MRM) pairs. Isotope-labeled internal standards and other internal standards were integrated in the Kit plate filter for metabolite quantification. The MxP500 Kit contained a 96 deep-well plate with a filter plate attached with sealing tape, and reagents and solvents used to prepare the plate assay. The first 14 wells in the Kit were used for one blank, three zero samples, seven standards and three quality control samples provided with each Kit. All the samples were analyzed with the Kit using the protocol described in the user manual. Briefly, samples were loaded onto the center of the filter on the upper 96-well kit plate and dried in a stream of nitrogen. Subsequently, 20 μL of a 5% solution of phenyl-isothiocyanate was added for derivatization. After incubation, the filter spots were dried again using an evaporator. Extraction of the metabolites was then achieved by adding 300 μL methanol containing 5 mM ammonium acetate. The extracts were obtained by centrifugation into the lower 96-deep well plate, followed by a dilution step with Kit MS running solvent. Mass spectrometric analysis was performed on an API5500 Qtrap® tandem mass spectrometry instrument (Applied Biosystems/MDS Analytical Technologies, Foster City, CA) equipped with a solvent delivery system. The samples were delivered to the mass spectrometer by a LC method followed by a direct injection method. The Biocrates MetIQ software was used to control the entire assay workflow, from sample registration to automated calculation of metabolite concentrations to the export of data into other data analysis programs. A targeted profiling scheme was used to quantitatively screen for known small molecule metabolites using multiple reaction monitoring, neutral loss and precursor ion scan.

2.11. Statistical analysis

All data were calculated as mean ± SEM followed by a t-test, non-parametric one-way or two-way ANOVA with Tukey's post-hoc test. Differences were considered statistically significant at $P < 0.05$. For metabolites, non-parametric one-way ANOVA with Tukey's post-hoc test was used to determine the statistical significance of the features. A false discovery rate (FDR) at a q-value of 0.05 was implemented to control multiple comparisons error. Metaboanalyst R version 5.0 was utilized to select the top 40 essential metabolites using Partial Least Square Discriminant Analysis (PLS-DA).[32] PLS-DA performance was tested with 5-fold cross-validation to avoid overfitting the training sets. At 5-fold cross-validation, R2 performance was more than 0.6 while Q2 was approximately 0.5. Top 26 metabolites were further selected with VIP scores of > 1.85 and < 2.20. A 2-D plot for principal components 1 and 2 was selected. In addition, Metaboanalyst R version 5.0 was used to compute a heatmap for sham, TAC, and TAC-A. Principal components analysis (PCA) biplot, heatmaps, and bar plots were computed and visualized using ggplot2 (V. 3.4.2; Wickham, 2016) package in R to evaluate the relative cytokine levels, gene expression, and cardiac remodeling as well as clusters restoring trend by ALY688 treatment and the relationship between the clusters variables. Quantitative enrichment analysis was performed with metaboanalyst to determine the association between TAC and TAC-A. For Biowire experiment, repeated measure two-way ANOVA with Tukey's or Sidak's post-hoc test was performed. Significance was determined with $p < 0.05$. For image analysis between two groups, a student's t-test was performed with significance at $p < 0.05$.

3. Results

3.1. ALY688 prevents TAC-induced HFrEF

To evaluate the preventive effect of ALY688 on TAC-induced cardiac dysfunction, a dose of 3 mg/kg of ALY688, chosen based on previous pharmacokinetic and pharmacodynamic studies, was administered via subcutaneous injection to mice 2 d prior to surgery and daily thereafter, as outlined in Fig. 1*A*. Cardiac function in all groups of animals was examined pre-study and then weekly using echocardiography. As expected, there was a gradual decrease in ejection fraction (EF) over 5 wk, yet this was significantly attenuated by ALY688 administration *(*Fig. 1*B&C)*. Assessing cardiac function in more detail after 5-wk of PO, indicated that ALY688 prevented PO-induced decreases in EF *(*Fig. 1*D)* and fractional shortening of the LV *(*Fig. 1*E)*. There was no significant change in cardiac output, although a trend towards an increase upon ALY688 administration *(*Fig. 1*F)*. Peak radial strain and peak longitudinal strain were compromised after 5 wk of PO and nominally recovered by ALY688, although there was no statistically significant change (Fig. 1*G, H*). Assessment of stroke volume, end-diastolic and -systolic volumes did not show statistically significant differences between the groups, except for elevated end-systolic volume after PO *(*Fig. 1*I-K)*. Finally, a significantly increased LV mass was observed in the TAC group, and this was prevented by ALY688 treatment (Fig. 1L), prompting us to next focus on alterations in hypertrophy. Additional data derived from echocardiography in each group throughout the duration of the study is presented in Supplementary Table 1. Overall, this data indicated that administration of ALY688 prevented TAC-induced cardiac dysfunction.

3.2. ALY688 attenuated adverse cardiac hypertrophic remodeling

We evaluated hypertrophy by measuring heart weight to body weight ratio *(*Fig. 2*A)*, circulating ANP levels *(*Fig. 2*B)*, and cardiomyocyte cross-sectional area determined by quantitative analysis of wheat germ agglutinin (WGA) staining of cardiac tissue sections *(*Fig. 2*C&D)*. The data collectively showed increased hypertrophic remodeling in mice following TAC surgery which was significantly reduced in mice that received daily ALY688 injections *(*Fig. 2*A-D)*. This correlates with the alterations in LV mass shown in Fig. 1*J*. Quantitative real-time PCR analysis demonstrated upregulation of several genes involved in myocardial hypertrophic remodeling, notably ANP and BNP, that were corrected by ALY688 *(*Fig. 2*E-G)*. Myosin heavy chain 6 (Myh 6) plus myosin light chain 2 and 3 (Myl2 and Myl3) content was decreased in mice after 5 wk of PO yet levels were maintained at similar levels to sham in mice administered ALY688 *(*Fig. 2*E-G)*. To find the relationships between the genes, a multivariate principal component analysis was performed on the dataset and summarized in a biplot graph *(*Fig. 2*F)*. The two main principal components capturing the highest variance in the data are shown on the x-axis (PCA1) and y-axis (PCA2). The vector's length and direction indicate the gene's contribution to variance in the PCAs. Longer vectors indicate genes with a stronger influence on the principal components, while shorter vectors indicate genes with less influence. Vectors that point in similar directions are positively correlated, while those pointing in opposite directions are negatively correlated, the bigger the angles, the lesser the correlation. The data points represent each mouse, with each treatment wrapped in an eclipse. Using this approach, we found separate clusters of TAC and TAC-A groups, while sham groups exhibited a dispersed distribution. Additionally, brain natriuretic peptide (BNP) had a strong influence on principal component 2 (PC2) clustering, and Myl3 strongly influenced PC1. Interestingly, Myh6 showed negative correlation with BNP, implying contrasting regulation of each in cardiac hypertrophy.

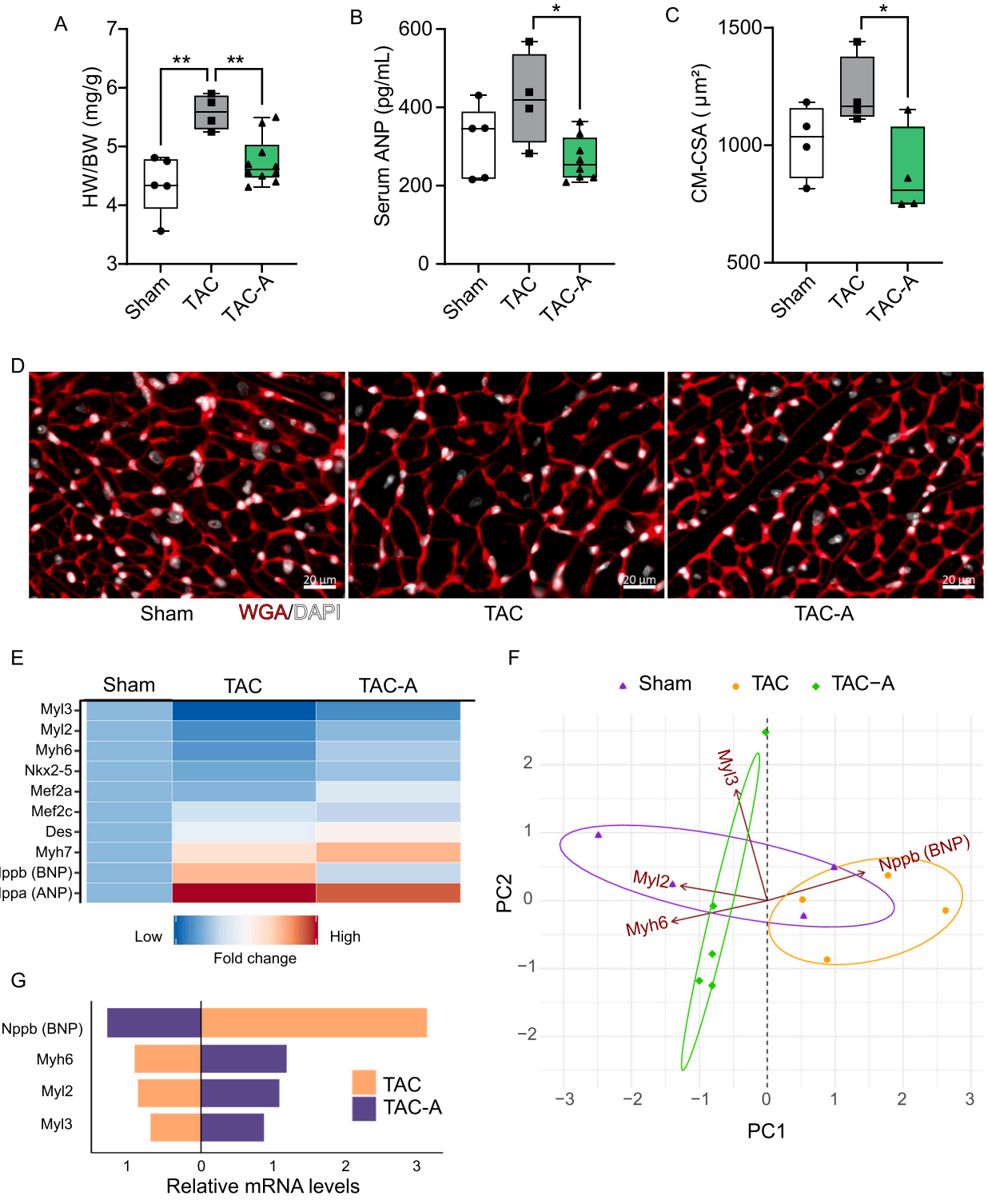

Fig. 2. ALY688 prevented adverse cardiac remodeling caused by pressure overload. (A) Heart weight to body weight ratio (HW/BW). (B) Serum atrial-natriuretic peptide (ANP). (C)Quantification of cardiomyocyte cross-sectional area (CM-CSA) (n=4 mice per group). (D) Representative fluorescent microscopy images of LV sections stained with wheat germ agglutinin (red: cardiomyocyte cell membrane) and DAPI (white: nuclei). (E) The heatmap of relative gene expression for genes related to cardiac hypertrophic remodeling (F) PCA biplot representing genes associated with cardiac hypertrophy. A point represents each mouse, with each group wrapped in an eclipse. Vectors with different length corresponding to importance and direction of each PC represent the gene expression. (G) The cluster of the expression of the genes related to cardiac hypertrophy shows restoring trend by ALY688. (H, I) Relative mRNA expression level of *Timp1* and *Nppb* gene normalized by *β-actin* expression. * = P<0.05, **=P<0.01. (n=5-10 mice per group).

3.3. ALY688 decreased TAC-induced myocardial fibrosis

We next assessed myocardial fibrosis using several well-established approaches. First, representative images of scanning electron microscopy of heart tissue for qualitative visualization of collagen fiber content and structural organization (Fig. 3*A*) showed areas of increased in collagen deposition (fibrosis) in the TAC group which was reduced by ALY688 administration. We then performed immunofluorescent analyses to detect alterations in the profile of hyper-secretory myofibroblasts. Concurrently, some desmin-expressing cardiomyocytes undergoing hypertrophic growth also express α-SMA, an actin isoform that is also expressed during early cardiomyocyte maturation. In Fig. 3*B*, fibroblasts are vimentin-only positive (green), and myofibroblasts are double-positive for α-SMA (blue) and vimentin. Data indicated little presence of α-SMA positive cells in the Sham group, except smooth muscle cells in vimentin/desmin/α-SMA triple-positive vessels, and wide-spread presence of vimentin/α-SMA double-positive myofibroblasts in the TAC group (Fig. 3*B*). α-SMA positive myofibroblasts were less prevalent in the ALY688 treated groups. ALY688 treated groups showed higher content and hypertrophy of vimentin-only-positive interstitial fibroblasts which are not fully activated into the contractile myofibroblast phenotype. The increased presence of hypertrophic fibroblasts and contractile myofibroblasts in the TAC group correlates with increased fibrosis observed in this group. The reduced presence of myofibroblasts in the treated groups supports findings of decreased fibrosis due to ALY688 treatment. To provide a more quantitative analysis of fibrosis, LV tissue sections isolated 5 wk post-surgery were stained with picrosirius red and revealed significantly increased collagen accumulation after TAC with an apparent reduction upon administration of ALY688 (Fig. 3*C&D*). Altered expression of several fibrosis-related genes was observed after 5 wk of PO (Fig. 3*E*). In particular, PO-induced increases in tissue inhibitor of matrix metalloproteinase (TIMP1), matrix metalloproteinase 3 (MMP3), periostin (Postn) and scleraxis (Scx) mRNA levels were prevented by ALY688 (Fig. 3*F*). Biplot analysis reinforced this conclusion and in particular the close relationship between scleraxis, periostin and TIMP1 (Fig. 3*G*).

To further investigate the effect of ALY688 on fibrosis, we used previously established heart-on-a-chip platform (Fig. 3*H*).[31] With ALY688 treatment (300 nM, every 2 days for 2 weeks), we measured the contractile force and dynamics of cardiac tissue, the expression of α-SMA, the ventricular isoform of the regulatory myosin light chain (MLC2v) with its alignment quantifications. The electrical properties of the tissues including excitation threshold (ET) and maximum capture rate (MCR) and other contractile parameters, such as passive tension, and beating duration were not significantly different between groups (*Supplementary Figure 1*). However, an increasing trend was observed in the active force of the ALY688-treated tissues (Fig. 3*I*). Moreover, the contractile slope (contraction velocity) and relaxation slope (relaxation velocity) (Fig. 3*J&K)* were significantly increased in the treatment group. Together with the reduced contraction time in the treated group (*Supplementary Figure 3D*), these results demonstrated cardiac contractile function improved with the treatment. In addition, the ALY688 treated tissues demonstrated a much lower α-SMA expression *(*Fig. 3*M)* and similar MLC2v expression *(Supplemental Figure G)* in comparison to the control tissues, evident by immunofluorescent detection. We also observed better MLC2v alignment in the untreated group, which can result from a more fibrotic, stiffer substrate. (Fig. 3*N*). Collectively, the data provide evidence of ALY688's beneficial effect on reducing cardiac fibrosis and the likely impact of this on cardiac functional performance.

3.4. ALY688 prevented alterations in various TAC-induced markers of inflammation

To assess the impact of ALY688 on TAC-induced changes in inflammatory factors, we first conducted an extensive analysis of the circulating level of 44 known inflammatory mediators using multiplex immunodetection (Fig. 4*A-C*). Of the tested targets, 34 fell within the detectable range of the assay (Fig. 4*A*). To explore the interplay between TAC and ALY688, or their reciprocal effects, a multivariate relationship analysis was performed. A group of cytokines, including interleukin-12 (IL-12p70), IL-17, IL-13, IL-15, IL-20, KC/CXCL1 (CXC motif chemokine ligand 1) and macrophage inflammatory proteins (MIP-1α, MIP-1b, MIP-3α (also known as chemokine ligand 20, CCL20), were detected at increased levels in response to TAC, but their elevation was prevented in the presence of ALY688 (Fig. 4*B&C)*. Our findings also revealed that 3 factors were decreased by TAC and prevented by ALY688; namely interleukin 1 alpha (IL-1α), macrophage-derived chemokine (MDC; CCL22) and erythropoietin (EPO), with strong positive correlations that can be explained by PC2 (Fig. 4*B&C*). Multivariate PC analysis biplot shows clustering of the different treatments wherein, although not fully separated, the clusters for sham/TAC-A are much closer than sham/TAC, suggesting that ALY688 treatment result in recovery for some genes that is closer to a normal body state. Nevertheless, cytokines usually play a more important role as paracrine factors although tissue levels may not correlate directly with circulating plasma levels we examined the expressions of inflammation-associated genes in the heart by quantitative real-time PCR analysis (Fig. 4*D-F*). We observed a positive correlation with *Pycard (*often referred to as ASC (Apoptosis-associated speck-like protein containing a CARD) and cluster of differentiation 247 (*Cd247)* genes, which exhibited low levels in TAC but were corrected by ALY688 administration. In contrast, *IL-6*, *IL-1β*, toll-like receptor 4 (*TLR4)* and heat shock protein 1 A (*Hspa1a)* genes showed an increasing trend after TAC which was corrected by ALY688. (Fig. 4*D-F*). Bar graphs and biplot indicated that vectors for genes, *IL-6, TLR4, IL-1β* and *Hspa1a*, were high in TAC, reversed in TAC-A and all lie in the x-axis negative part of the graph with closer cosine angles indicating a positive correlation among these genes. On the contrary, genes *Pycard* and *Cd247* with high TAC levels, reversed in TAC-A, lie in the positive x-axis, exhibit a stronger positive correlation, and show a negative correlation with genes such as *Hspa1a* and *TLR4*. Overall, this analysis demonstrates that ALY688 attenuates pro-inflammatory changes induced by PO in mice.

3.5. ALY688 altered cardiac metabolomic profile in mice with and without TAC

Analysis of data from targeted metabolomics conducted by LC-MS/MS (liquid chromatography-mass spectrometry), indicated a distinct separation in the metabolic profiles of each group of mice (Fig. 5*A*). Among the top 40 significantly altered metabolites, the first obvious alteration is an overall trend towards lower levels of TG in the TAC-A group, while the TAC group exhibited intermediate levels (Fig. 5*B&C*). Likewise, in comparing TAC versus TAC-A functional enrichment results, the largest differential effect involved numerous categories related to mitochondrial beta-oxidation of fatty acids was a highly prominent feature (Fig. 5*D*). These findings support the adiponectin-like effect of ALY688 on cardiac metabolism, specifically in promoting fatty acid mobilization and utilization.

4. Discussion

Treatments for various forms of heart failure continue to emerge, yet it is still imperative to expand our therapeutic arsenal *[6,7]*. In particular, this study was designed to test the therapeutic potential of an adiponectin agonist which we proposed would be cardioprotective in a preclinical model of heart failure with reduced ejection fraction (HFrEF). Ideally, a tailored therapy for patients with HFrEF would encompass contributory factors to HF severity such as insulin resistance, metabolic inflexibility, hypertrophy, inflammation and fibrosis [33]. Previous studies have established that recombinant or adenoviral-delivered adiponectin regulates these processes and confers cardioprotective effects [11,12,34]. Many attempts have been made to develop adiponectin-based therapeutics since use of recombinant

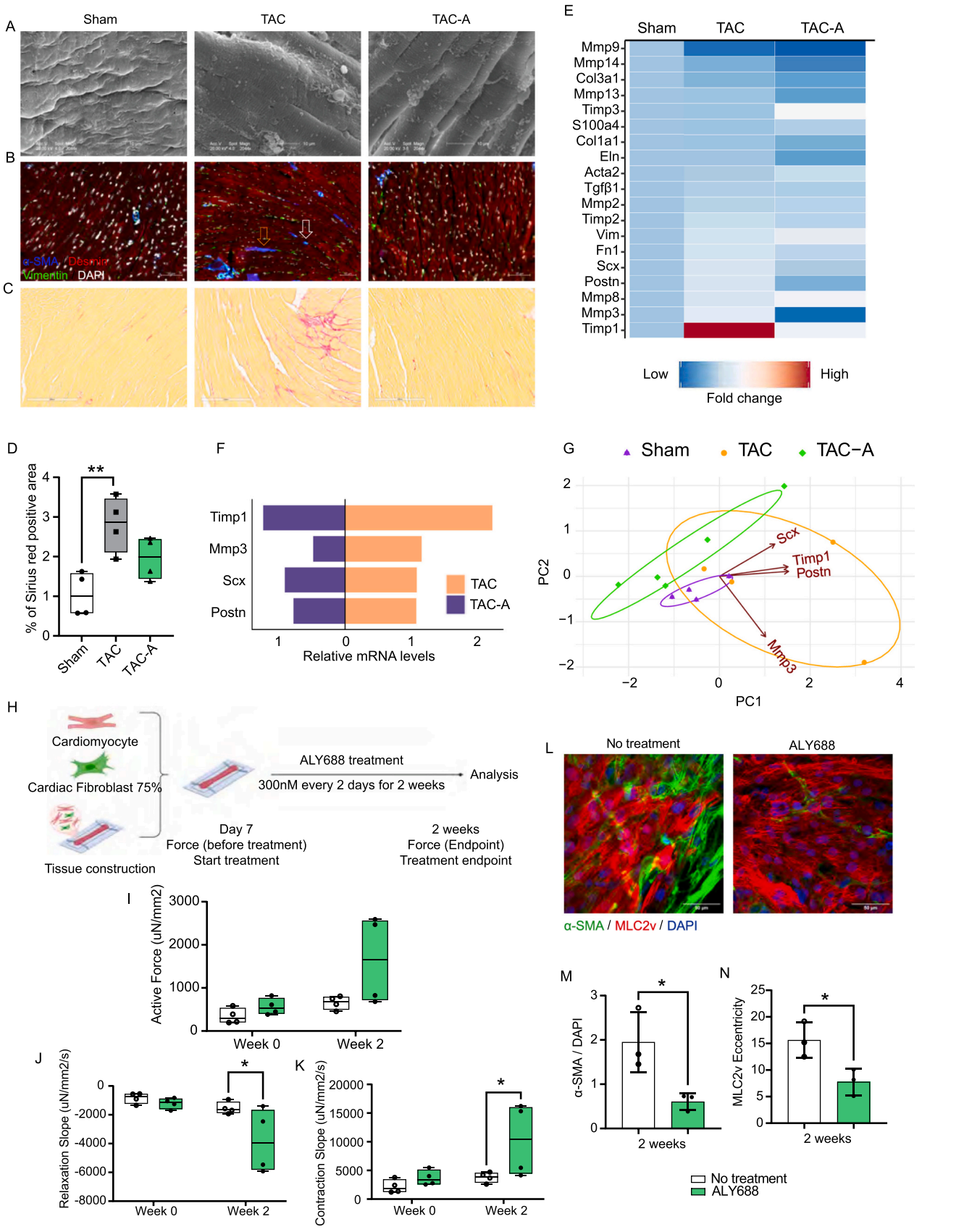

(caption on next page)

Fig. 3. ALY688 attenuated cardiac fibrosis. (A) Representative scanning electron microscopy images of LV samples isolated 5 wk post surgery shown at 2044X. Right column images have been zoomed to show structural features of interest. (B) Representative images of Picosirius red staining of heart section and (C) the quantitation of % of positive Picosirius red area. (D) Immunofluorescent detection of individual cell types within the LV 5 wk post-surgery. Representative images show desmin (red), α-SMA (blue), vimentin (green), and nuclei (white, DAPI). White arrow points to an α-SMA-positive / desmin-negative myofibroblast and the yellow arrow indicates an α-smooth muscle actin-, desmin-double positive cardiomyocyte. Vascular structures are triple- positive for α-SMA and desmin (smooth muscle cells) and vimentin (endothelial cells). Fibroblasts are vimentin-only positive (green), and myofibroblasts are double-positive for α-SMA and vimentin. Scale bar: 20 μm. (E) The heatmap of relative gene expression for genes related to cardiac fibrotic remodeling. (F) The cluster of the expression of the genes related to cardiac fibrosis shows restoring trend by ALY688. (G) PCA biplot representing genes associated with cardiac fibrosis. (H) Schematic of tissue construction and treatment regimen (I) Active forces of tissues stimulated at 1 Hz; (J) Relaxation slope and (K) Contraction slope during tissue beating; (L) Representative immunostaining images of treated and control tissues at treatment endpoint stained for α-SMA (green), ventricular myosin light chain-2 (MLC2v, red) and counterstained with DAPI (blue) (M) Normalized expression level of α-SMA over DAPI (N) Eccentricity analysis of sarcomere alignment based on MLC2v staining.

adiponectin itself is limited by several factors such as the large size and requirement for complex post-translational modifications to ensure bioactivity [35]. To overcome this, Otvos and colleagues identified the receptor binding domain mediating activity and generated the small peptide adiponectin mimetic ADP355 [25]. This structure was further optimized by identifying non-critical amino acids and modification with non-natural amino acids to develop an optimal size and configuration. The resulting peptide, ALY688, was found to activate both AdipoR1 and AdipoR2 more potently than the original peptide, while also being more resistant to degradation [36]. Furthermore, a sustained release (SR) formulation of the peptide developed for subcutaneous administration was used in this study. Animals received daily administration of 3 mg/kg ALY688 two days before and throughout the course of five weeks after TAC.

Importantly, weekly echocardiography to assess cardiac function indicated that ALY688 administration conferred significant functional beneficial effects. This is the first study to demonstrate that treatment with this adiponectin-mimetic peptide can attenuate the reduction in EF associated with pressure overload. In general terms, this establishes ALY688 as a potential therapeutic intervention in cases of HFrEF. ALY688 has progressed through multiple preclinical studies, including toxicology and is poised to enter phase I clinical trials.

To gain insight into the mechanisms underlying the beneficial effect of ALY688 on cardiac function, we examined well established cardiac remodeling events known to occur after TAC [37,38]. First, LV hypertrophy is commonly observed in cases of HFrEF or diabetic cardiomyopathy and is a strong predictor of adverse cardiovascular outcomes, such that regression of LV hypertrophy reduces cardiovascular morbidity and mortality.[39] Reduced hypertrophy can be achieved via use of anti-hypertensive agents, although not all patients exhibit regression of LV hypertrophy after treatment [40]. PO-induced hypertrophy is exaggerated in adiponectin knockout mice and can be attenuated by adiponectin administration [15,21,41,42]. In our study, indices of hypertrophy showed the expected increase after TAC. These included LV mass determined by echocardiography, heart weight to body weight ratio, cardiomyocyte cross sectional area, as well as ANP and BNP levels. Across these measures, ALY688 reduced the extent of hypertrophy. Previous studies have shown that adiponectin has anti-hypertrophic effects and our data indicate that ALY688 mimics this beneficial response [43,44]. Interestingly, our data also indicated that ALY688 prevented alterations in Myh6 plus Myl2 and Myl3 content after TAC, all of which have been implicated in cardiomyopathy [45,46]. Collectively, these data are of great interest in light of the current interest in therapeutic myosin modulators to target cardiac myosins directly and improve contractility and cardiac power output in dilated and hypertrophic cardiomyopathies [47]. In summary, this anti-hypertrophic aspect of ALY688 action may be an important mechanistic component for effective intervention to improve outcomes in at-risk patients.

Fibrosis is a major consequence of PO and previous studies have established that this is exaggerated in adiponectin knockout mice and can be reduced by adiponectin [15,27,42]. Here, we observed that treatment with ALY688 resulted in a reduction in PO-induced fibrosis. Notably, ALY688-treated mice exhibited decreased αSMA content in stress fibers and reduced collagen deposition. Analysis of alterations in mRNA levels of fibrosis related genes provided interesting mechanistic insight. For example, the myofibroblast profile change we observed may be related to increased expression of the transcription factor scleraxis after PO and its correction by ALY688. Myocardial scleraxis expression has been shown to be upregulated in mice after PO and in non-ischemic dilated cardiomyopathy patients [48]. It regulates cardiac fibroblast activation and scleraxis knockout attenuated fibrosis and improved cardiac function after PO, thus has been proposed as a viable target for the development of novel anti-fibrotic treatments [48–50]. Periostin is a myofibroblast marker induced by scleraxis which we also observed to be elevated after TAC and attenuated by ALY688 [48]. Periostin is commonly used as a biomarker of fibrotic remodeling, as a cause of increased heart failure susceptibility and as potentially useful drug target [51]. We also observed that ALY688 corrected PO-induced elevation in tissue inhibitor of matrix metalloproteinase-1 levels, which has strong implications for fibrotic remodeling [52,53]. To further validate the anti-fibrotic effect of ALY688, we employed an organ-on-chip system [54,55]. Our results demonstrated that ALY688 treatment attenuated the expression of α-SMA and improved cardiac contractility, indicated by a trend of stronger active force, and significantly faster contraction and relaxation of the cardiac tissues. It is important to emphasize that an increasing trend in active force with large fold changes at a tissue level is rare in the previously reported anti-fibrosis treatment [56]. These findings collectively indicate potent anti-fibrotic properties of ALY688 in the context of stress conditions, such as PO.

In various models of heart failure, inflammation plays a fundamentally important role in driving adverse cardiac remodeling and can be closely associated with hypertrophic and fibrotic changes [57,58]. Adiponectin has been shown to have anti-inflammatory effects via numerous mechanisms [59]. Our study found that ALY688 regulated basal or PO-induced alterations in the level of numerous pro- or anti-inflammatory factors. Elevated circulating levels of factors that have been suggested to contribute to the pathogenesis of inflammatory diseases, such as IL-5, IL-13 and IL-17, after 5 wk of PO were prevented by ALY688 [60]. For example, IL-13 levels are elevated in patients with chronic heart failure [61]. IL-5 and IL-13 were inversely correlated with responsiveness of heart failure patients to left ventricular assist device intervention [62]. Previous research has shown that plasma IL-12 concentrations are significantly increased in patients with cardiovascular diseases and targeting IL-12 in murine heart failure models alleviated cardiac dysfunction [63–65]. IL-17 induction occurs in late remodeling stages (28 d after PO) and mediates sustained infiltration of immune cells and their production of pro-inflammatory cytokines, enhanced fibroblast proliferation, and increased expression of profibrotic genes. Additionally, TAC mice exhibited significantly higher levels of MIP-3α (macrophage inflammatory protein-3 alpha, also known as CCL20) in circulation which is a biomarker for heart failure patients [66,67]. MIP-3α has been shown to be involved in TNF-α-mediated signaling pathways in human cardiac fibroblasts, potentially leading to inflammatory responses [68]. The chemo attractants MCP-1, MIP-1β, MIP-1α and MIP-3α followed a similar change in expression pattern, all with potential significance in determining cardiac function [69]. Direct assessment of myocardial transcript levels for inflammatory-related

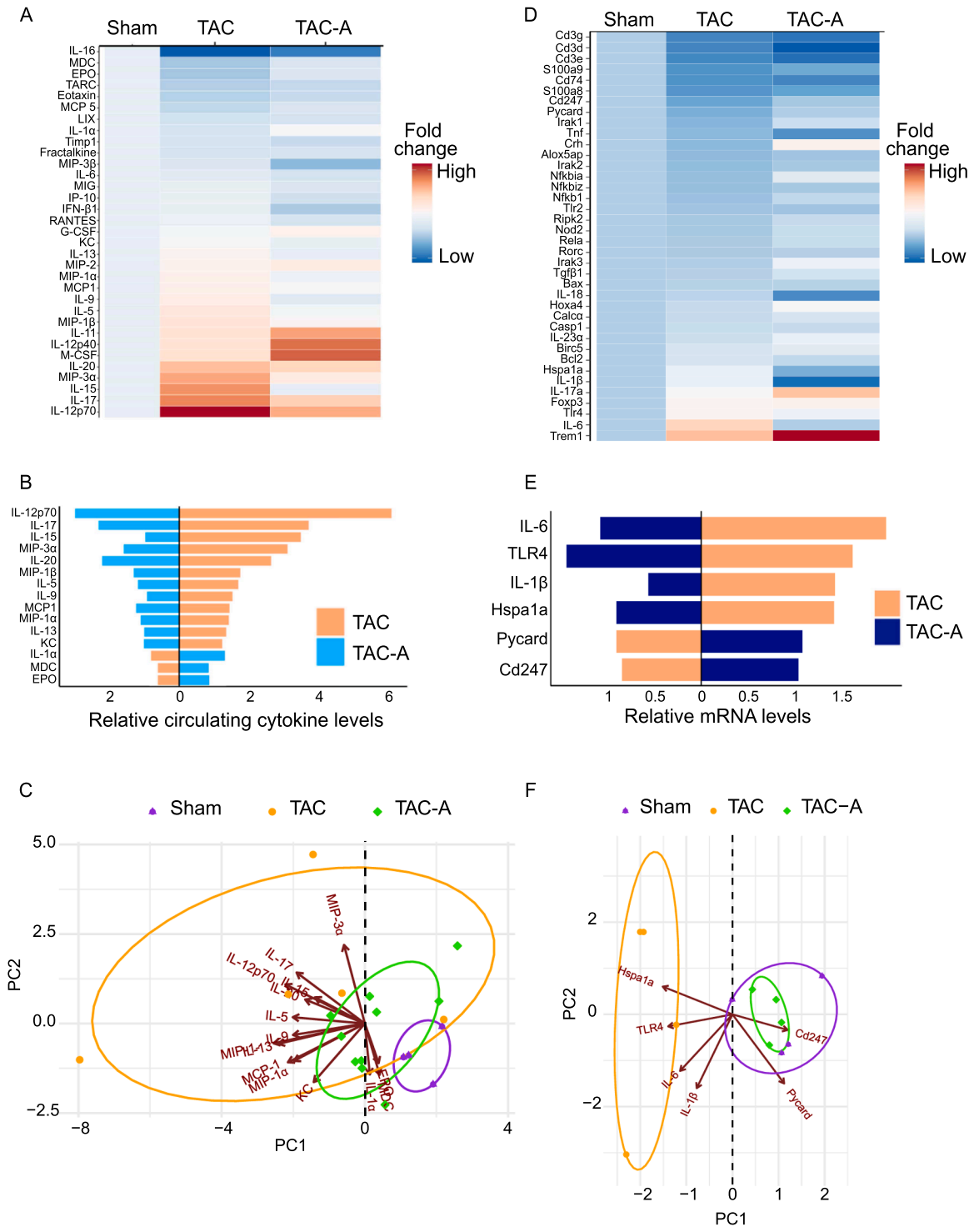

Fig. 4. ALY688 regulated PO-induced inflammatory phenotype. (A) The heatmap of relative cytokine levels in the serum of mice. (B) The cluster of cytokines showed restoring trend by ALY688, the orange bar: TAC, the blue bar: TAC-A. (C) The biplot of 44 circulating cytokine levels. A point represents each mouse, with each group wrapped in an eclipse. Vectors with different lengths corresponding to importance and direction of each PC represent the gene expression. (D) The heatmap of relative mRNA expression of inflammatory genes in heart tissue. (E) The cluster of cytokines showed restoring trend by ALY688, the orange bar: TAC, the cobalt blue bar: TAC-A. (F) The biplot of gene expressions related to inflammation.

genes also provided new insight on mechanisms of ALY688 action. There was attenuation of the PO-induced elevations in IL-6, TLR-4 and IL-1b. IL-6 levels typically increase in patients with heart failure and a recent study showed that attenuating PO-induced increases in IL-6 with raloxifene can improve cardiac function [70,71]. These are likely to confer important beneficial effects on heart failure given our current knowledge on the role of inflammasome activation in various models of heart failure and the success of anti-IL-1b therapeutics [72,73]. Somewhat surprisingly given these changes in IL-1β and TLR4, the level of PYCARD gene which encodes apoptosis-associated speck-like protein containing a CARD (ASC) that is important in inflammasome formation was reduced after PO and elevated by ALY688 [72]. Hspa1a is a key

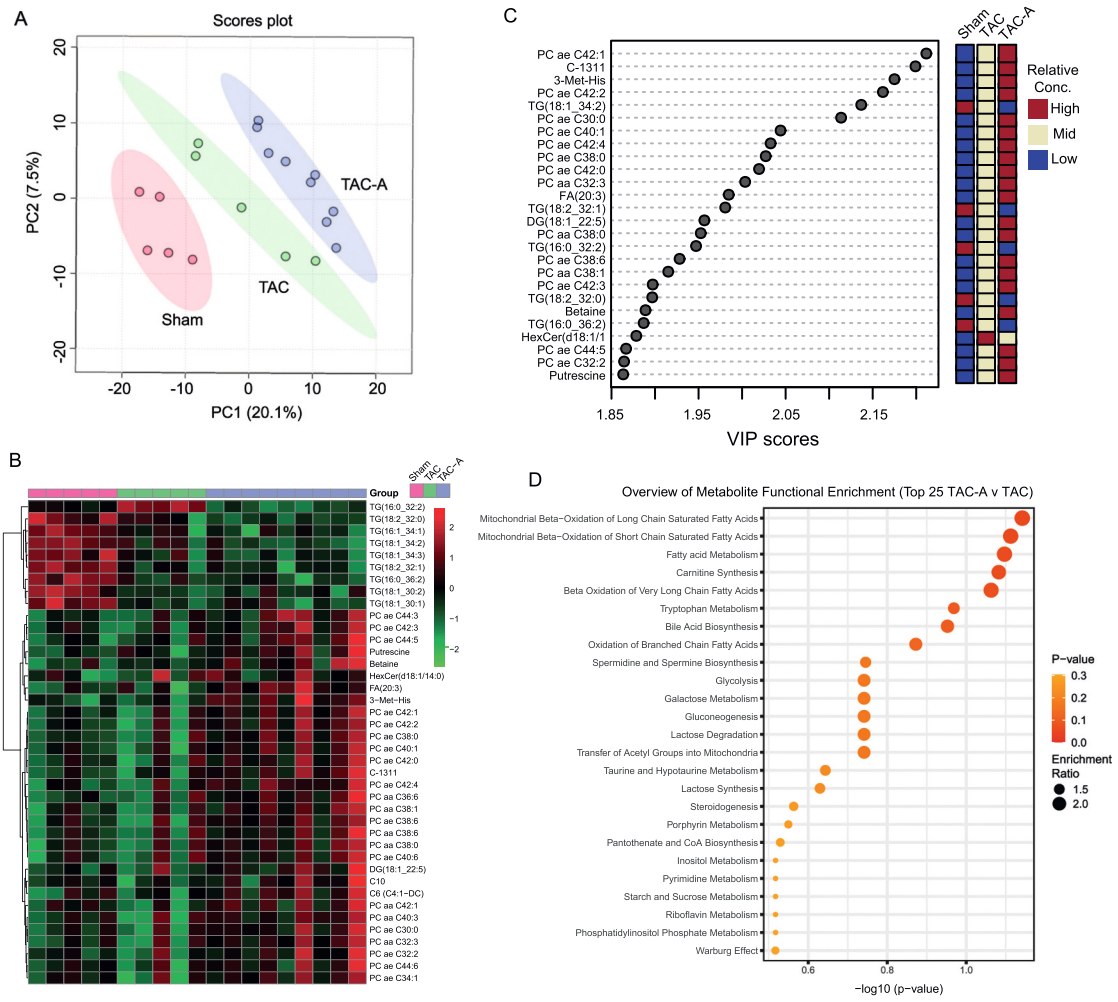

Fig. 5. ALY688 affects to metabolic profile of PO hearts. Targeted metabolomic analysis was conducted with heart tissue at 5 wk post-surgery. (A) Score plot of metabolic profile from all heart tissue samples using PLS-DA model. (B) Heatmap analysis of 40 significant metabolites, as identified by VIP scores in PLS-DA analysis. The different groups of sham, TAC, and TAC-a were indicated in blue, gold and purple respectively. The red color represents the trend in increase, and green represents a decrease. (C) PLS-DA variable importance plot of top 26 metabolites with the highest discriminatory power in the treatment groups. Red field show a high abundance, blue fields a low abundance of the listed row-wise metabolites based on the different groups. (D) Metabolite Set Enrichment Analysis (MSEA) of metabolites perturbed when comparing TAC and TAC-A shown in decreasing order of enrichment. Color intensity shows the significance level, with darker colors representing higher significance. Dot size indicates the enrichment ratio, the bigger the size, the higher the enrichment ratio.

member of the 70-kDa heat shock protein (Hsp70) family of molecular chaperones that are expressed in response to various stressors to protect the heart [74]. The fact that no increase in Hspa1a was seen after TAC in mice treated with ALY688 suggests an early cardioprotective effect of the peptide that negates the endogenous stimulus for Hspa1a expression. In summary, our data portray effects of ALY688 on a range of targets that would confer anti-inflammatory outcomes.

Metabolic dysregulation is recognized as a primary driver and significant contributing factor in the development of heart failure after TAC [4,33]. Clinical studies have shown that interventions aimed at modifying myocardial energy metabolism can lead to improved clinical outcomes in heart failure patients, and there is growing evidence linking adiponectin signaling to favorable metabolic profiles in these studies [4, 75]. In our study, we investigated metabolic alterations in the heart using targeted metabolomics and PLS-DA analysis indicated clear distinction of metabolite profiles between sham, TAC and TAC-A groups. Foremost was an effect of ALY688 on reducing myocardial lipids, particularly triglycerides. This reduction could be attributed to the direct regulation of lipid metabolism enzymes or potentially as a secondary effect of increased mitochondrial fatty acid oxidation. The promotion of fatty acid oxidation induced by ALY688 may be a consequence of the activation of cardiac AMP-activated protein kinase (AMPK), which is known to stimulate fatty acid oxidation in the heart and is a well-established target of adiponectin action [4,76]. We observed an increase in PCs following ALY688 administration. PCs are major structural lipids in the plasma membrane, and their metabolism by intestinal microbes results in the production of choline and betaine. As betaine has been reported to relieve hepatic inflammation and improve insulin sensitivity in NASH, and was found to be elevated here, it may represent a new axis of adiponectin action upon cardiac metabolism [77]. Furthermore, betaine is converted to trimethylamine N-oxide (TMAO) and the positive correlation between increased TMAO levels and the risk of CVD has been reported [78]. Another amino acid, putrescine, was increased by ALY688 treatment in mice hearts. Putrescine has been reported to exert cardioprotective effects via resolving inflammation [79]. Furthermore, it has been established that spermidine is produced from putrescine, and previous studies have reported that spermidine exerts a cardioprotective effect through an autophagy-dependent mechanism [80]. While revealing the cardioprotective effect of ALY688 and potential mechanisms of action, statistical power in this study was limited by a relatively low number of mice (5 to 9 per group). Overall, it is plausible that the favorable effects of ALY688 on cardiac function, hypertrophy, inflammation and fibrosis in failing hearts arise from a synergistic modulation of the metabolic function, in particular favoring

mitochondrial fatty acid metabolism.

There are also several potential limitations of the study which we are aware of. We did not include a study arm with sham-operated animals following treatment with ALY688. Molecular analyses were performed at termination of the study and it is possible there are secondary effects that might exist based on differences in contractile function. It would be advantageous to perform another follow up study using AdipoR1/2 knockout mice in order to further verify the specificity of ALY688 action, as has been done in cellular models [81]. We observed no change in circulating adiponectin levels between groups in this study yet analysis of myocardial AdipoR expression may be of value. Finally, a higher number of animals in each group would potentially allow current trends in data to become statistically significant.

In summary, we show that ALY688 attenuates the development of cardiac dysfunction induced by PO and that underlying this favourable outcome are beneficial metabolic, anti-inflammatory, anti-hypertrophic and anti-fibrotic effects on the myocardium. Accordingly, this work identifies ALY688 as a promising therapeutic agent for cases of HFrEF and likely other types of heart failure.

CRediT authorship contribution statement

Zhao Yimu: Investigation, Methodology, Writing – review & editing. **Cheung Krisco:** Data curation, Formal analysis, Investigation. **Mirzaesmaeili Ali:** Investigation. **Noskovicova Nina:** Investigation. **Radisic Milica:** Resources, Supervision, Visualization. **Hinz Boris:** Investigation, Methodology, Writing – review & editing. **Sater Ali Abdul:** Investigation, Supervision. **Sweeney Gary:** Conceptualization, Funding acquisition, Project administration, Supervision, Writing – review & editing. **Sung Hye Kyoung:** Data curation, Formal analysis, Investigation, Supervision. **Ayansola Oyeronke:** Formal analysis, Visualization. **Hsu Henry H.:** Conceptualization, Project administration, Resources, Writing – review & editing. **Cho Sungji:** Data curation, Formal analysis, Investigation, Writing – review & editing. **Lopaschuk Gary D:** Formal analysis, Writing – review & editing. **Dadson Keith:** Data curation, Formal analysis, Investigation, Methodology, Writing – original draft.

Declaration of Competing Interest

The authors declare the following financial interests/personal relationships which may be considered as potential competing interests: HHH is the CEO and GS and AAS act as consultants for Allysta Pharmaceuticals Inc. MR and YZ are inventors on a patent licenced to Valo Health and are receiving licencing revenue from this invention.

Data availability

Data will be made available on request.

Acknowledgements

GS acknowledges research support from Canadian Institutes of Health Research and Heart & Stroke Foundation of Canada. HKS acknowledges Fellowship support from Canadian Institutes of Health Research. The research of BH is supported by a foundation grant from the Canadian Institutes of Health Research (#375597) and support from the John Evans Leadership funds (#36050, #38861, and #38430) and innovation funds (Fibrosis Network, #36349) from the Canada Foundation for Innovation (CFI) and the Ontario Research Fund (ORF). Canadian Institutes of Health Research (CIHR) Foundation Grant FDN-167274, Canada Foundation for Innovation/Ontario Research Fund grant 36442. MR was supported by Canada Research Chairs and Killam Fellowship. YZ is supported by CIHR Post-doctoral Fellowship. We thank Dr Kristin Schram for preparing the graphic abstract.

Appendix A. Supporting information

Supplementary data associated with this article can be found in the online version at doi:10.1016/j.biopha.2023.116119.

References

[1] E.J. Benjamin, P. Muntner, A. Alonso, M.S. Bittencourt, C.W. Callaway, A. P. Carson, A.M. Chamberlain, A.R. Chang, S. Cheng, S.R. Das, F.N. Delling, L. Djousse, M.S.V. Elkind, J.F. Ferguson, M. Fornage, L.C. Jordan, S.S. Khan, B. M. Kissela, K.L. Knutson, T.W. Kwan, D.T. Lackland, T.T. Lewis, J.H. Lichtman, C. T. Longenecker, M.S. Loop, P.L. Lutsey, S.S. Martin, K. Matsushita, A.E. Moran, M. E. Mussolino, M. O'Flaherty, A. Pandey, A.M. Perak, W.D. Rosamond, G.A. Roth, U. K.A. Sampson, G.M. Satou, E.B. Schroeder, S.H. Shah, N.L. Spartano, A. Stokes, D. L. Tirschwell, C.W. Tsao, M.P. Turakhia, L.B. VanWagner, J.T. Wilkins, S.S. Wong, S.S. Virani, Heart Disease and Stroke Statistics-2019 Update: A Report From the American Heart Association, Circulation 139 (10) (2019) e56-e528.

[2] K. Dadson, V. Kovacevic, P. Rengasamy, G.H. Kim, S. Boo, R.K. Li, I. George, P. C. Schulze, B. Hinz, G. Sweeney, Cellular, structural and functional cardiac remodelling following pressure overload and unloading, Int J. Cardiol. 216 (2016) 32–42.

[3] Y.K. Tham, B.C. Bernardo, J.Y. Ooi, K.L. Weeks, J.R. McMullen, Pathophysiology of cardiac hypertrophy and heart failure: signaling pathways and novel therapeutic targets, Arch. Toxicol. 89 (9) (2015) 1401–1438.

[4] G.D. Lopaschuk, Q.G. Karwi, R. Tian, A.R. Wende, E.D. Abel, Cardiac Energy Metabolism in Heart Failure, Circ. Res 128 (10) (2021) 1487–1513.

[5] G.H. Kim, N. Uriel, D. Burkhoff, Reverse remodelling and myocardial recovery in heart failure, Nat. Rev. Cardiol. 15 (2) (2018) 83–96.

[6] M. Gheorghiade, C.J. Larson, S.J. Shah, S.J. Greene, J.G. Cleland, W.S. Colucci, P. Dunnmon, S.E. Epstein, R.J. Kim, R.V. Parsey, N. Stockbridge, J. Carr, W. Dinh, T. Krahn, F. Kramer, K. Wahlander, L.I. Deckelbaum, D. Crandall, S. Okada, M. Senni, S. Sikora, H.N. Sabbah, J. Butler, Developing New Treatments for Heart Failure: Focus on the Heart, Circ. Heart Fail 9 (5) (2016).

[7] P. Rossignol, A.F. Hernandez, S.D. Solomon, F. Zannad, Heart failure drug treatment, Lancet 393 (10175) (2019) 1034–1044.

[8] S.C. da Silva Rosa, M. Liu, G. Sweeney, Adiponectin synthesis, secretion and extravasation from circulation to interstitial space, Physiol. (Bethesda) 36 (3) (2021) 134–149.

[9] M. Ryo, T. Nakamura, S. Kihara, M. Kumada, S. Shibazaki, M. Takahashi, M. Nagai, Y. Matsuzawa, T. Funahashi, Adiponectin as a biomarker of the metabolic syndrome, Circ. J. 68 (11) (2004) 975–981.

[10] Y. Iwashima, T. Katsuya, K. Ishikawa, N. Ouchi, M. Ohishi, K. Sugimoto, Y. Fu, M. Motone, K. Yamamoto, A. Matsuo, K. Ohashi, S. Kihara, T. Funahashi, H. Rakugi, Y. Matsuzawa, T. Ogihara, Hypoadiponectinemia is an independent risk factor for hypertension, Hypertension 43 (6) (2004) 1318–1323.

[11] R. Shibata, Y. Izumiya, K. Sato, K. Papanicolaou, S. Kihara, W.S. Colucci, F. Sam, N. Ouchi, K. Walsh, Adiponectin protects against the development of systolic dysfunction following myocardial infarction, J. Mol. Cell Cardiol. 42 (6) (2007) 1065–1074.

[12] R. Shibata, K. Sato, D.R. Pimentel, Y. Takemura, S. Kihara, K. Ohashi, T. Funahashi, N. Ouchi, K. Walsh, Adiponectin protects against myocardial ischemia-reperfusion injury through AMPK- and COX-2-dependent mechanisms, Nat. Med 11 (10) (2005) 1096–1103.

[13] Z.V. Wang, P.E. Scherer, Adiponectin, the past two decades, J. Mol. Cell Biol. 8 (2) (2016) 93–100.

[14] J.L. Parker-Duffen, K. Walsh, Cardiometabolic effects of adiponectin, Best. Pr. Res Clin. Endocrinol. Metab. 28 (1) (2014) 81–91.

[15] N. Zhang, W.Y. Wei, H.H. Liao, Z. Yang, C. Hu, S.S. Wang, W. Deng, Q.Z. Tang, AdipoRon, an adiponectin receptor agonist, attenuates cardiac remodeling induced by pressure overload, J. Mol. Med (Berl.) 96 (12) (2018) 1345–1357.

[16] C. Ren, W. Yi, B. Jiang, E. Gao, J. Liang, B. Zhang, Z. Yang, D. Zheng, Y. Zhang, Diminished AdipoR1/APPL1 Interaction Mediates Reduced Cardioprotective Actions of Adiponectin against Myocardial Ischemia/Reperfusion Injury in Type-2 Diabetic Mice, Stem Cells Int 2023 (2023) 7441367.

[17] A. Sharma, M. Mah, R.H. Ritchie, M.J. De, Blasio, The adiponectin signalling pathway - A therapeutic target for the cardiac complications of type 2 diabetes? Pharm. Ther. 232 (2022) 108008.

[18] Y. Kim, J.H. Lim, E.N. Kim, Y.A. Hong, H.J. Park, S. Chung, B.S. Choi, Y.S. Kim, J. Y. Park, H.W. Kim, C.W. Park, Adiponectin receptor agonist ameliorates cardiac lipotoxicity via enhancing ceramide metabolism in type 2 diabetic mice, Cell Death Dis. 13 (3) (2022) 282.

[19] A. Jenke, M. Yazdanyar, S. Miyahara, A. Chekhoeva, M.B. Immohr, J. Kistner, U. Boeken, A. Lichtenberg, P. Akhyari, AdipoRon Attenuates Inflammation and Impairment of Cardiac Function Associated With Cardiopulmonary Bypass-Induced Systemic Inflammatory Response Syndrome, J. Am. Heart Assoc. 10 (6) (2021) e018097.

[20] Y. Zhang, J. Zhao, R. Li, W.B. Lau, Y.X. Yuan, B. Liang, R. Li, E.H. Gao, W.J. Koch, X.L. Ma, Y.J. Wang, AdipoRon, the first orally active adiponectin receptor activator, attenuates postischemic myocardial apoptosis through both AMPK-mediated and AMPK-independent signalings, Am. J. Physiol. Endocrinol. Metab. 309 (3) (2015) E275–E282.

[21] K.M. O'Shea, D.J. Chess, R.J. Khairallah, S. Rastogi, P.A. Hecker, H.N. Sabbah, K. Walsh, W.C. Stanley, Effects of adiponectin deficiency on structural and

metabolic remodeling in mice subjected to pressure overload, Am. J. Physiol. Heart Circ. Physiol. 298 (6) (2010) H1639–H1645.
[22] H.K. Sung, P.L. Mitchell, S. Gross, A. Marette, G. Sweeney, ALY688 elicits adiponectin-mimetic signaling and improves insulin action in skeletal muscle cells, Am. J. Physiol. Cell Physiol. 322 (2) (2022) C151–C163.
[23] D. Da Eira, S. Jani, H. Sung, G. Sweeney, R.B. Ceddia, Effects of the adiponectin mimetic compound ALY688 on glucose and fat metabolism in visceral and subcutaneous rat adipocytes, Adipocyte 9 (1) (2020) 550–562.
[24] P. Kumar, T. Smith, K. Rahman, N.E. Thorn, F.A. Anania, Adiponectin agonist ADP355 attenuates CCl4-induced liver fibrosis in mice, PLoS One 9 (10) (2014) e110405.
[25] L. Otvos Jr., I. Kovalszky, J. Olah, R. Coroniti, D. Knappe, F.I. Nollmann, R. Hoffmann, J.D. Wade, S. Lovas, E. Surmacz, Optimization of adiponectin-derived peptides for inhibition of cancer cell growth and signaling, Biopolymers 104 (3) (2015) 156–166.
[26] F.S. Younesi, D.O. Son, J. Firmino, B. Hinz, Myofibroblast Markers and Microscopy Detection Methods in Cell Culture and Histology, Methods Mol. Biol. 2299 (2021) 17–47.
[27] K. Dadson, S. Turdi, S. Boo, B. Hinz, G. Sweeney, Temporal and Molecular Analyses of Cardiac Extracellular Matrix Remodeling following Pressure Overload in Adiponectin Deficient Mice, PLoS One 10 (4) (2015) e0121049.
[28] Y. Zhao, E.Y. Wang, L.H. Davenport, Y. Liao, K. Yeager, G. Vunjak-Novakovic, M. Radisic, B. Zhang, A Multimaterial Microphysiological Platform Enabled by Rapid Casting of Elastic Microwires, Adv. Health Mater. 8 (5) (2019) e1801187.
[29] X. Lian, J. Zhang, S.M. Azarin, K. Zhu, L.B. Hazeltine, X. Bao, C. Hsiao, T.J. Kamp, S.P. Palecek, Directed cardiomyocyte differentiation from human pluripotent stem cells by modulating Wnt/beta-catenin signaling under fully defined conditions, Nat. Protoc. 8 (1) (2013) 162–175.
[30] Y. Zhao, N. Rafatian, N.T. Feric, B.J. Cox, R. Aschar-Sobbi, E.Y. Wang, P. Aggarwal, B. Zhang, G. Conant, K. Ronaldson-Bouchard, A. Pahnke, S. Protze, J.H. Lee, L. Davenport Huyer, D. Jekic, A. Wickeler, H.E. Naguib, G.M. Keller, G. Vunjak-Novakovic, U. Broeckel, P.H. Backx, M. Radisic, A Platform for Generation of Chamber-Specific Cardiac Tissues and Disease Modeling, Cell 176 (4) (2019) 913–927, e18.
[31] Y. Zhao, N. Rafatian, E.Y. Wang, N.T. Feric, B.F.L. Lai, E.J. Knee-Walden, P. H. Backx, M. Radisic, Engineering microenvironment for human cardiac tissue assembly in heart-on-a-chip platform, Matrix Biol. 85-86 (2020) 189–204.
[32] Z. Pang, G. Zhou, J. Ewald, L. Chang, O. Hacariz, N. Basu, J. Xia, Using MetaboAnalyst 5.0 for LC-HRMS spectra processing, multi-omics integration and covariate adjustment of global metabolomics data, Nat. Protoc. 17 (8) (2022) 1735–1761.
[33] S. Sankaralingam, G.D. Lopaschuk, Cardiac energy metabolic alterations in pressure overload-induced left and right heart failure (2013 Grover Conference Series), Pulm. Circ. 5 (1) (2015) 15–28.
[34] H. Li, W. Yao, Z. Liu, A. Xu, Y. Huang, X.L. Ma, M.G. Irwin, Z. Xia, Hyperglycemia Abrogates Ischemic Postconditioning Cardioprotection by Impairing AdipoR1/Caveolin-3/STAT3 Signaling in Diabetic Rats, Diabetes 65 (4) (2016) 942–955.
[35] Y. Liu, V. Vu, G. Sweeney, Examining the Potential of Developing and Implementing Use of Adiponectin-Targeted Therapeutics for Metabolic and Cardiovascular Diseases, Front Endocrinol. (Lausanne) 10 (2019) 842.
[36] L. Otvos Jr., D. Knappe, R. Hoffmann, I. Kovalszky, J. Olah, T.D. Hewitson, R. Stawikowska, M. Stawikowski, P. Cudic, F. Lin, J.D. Wade, E. Surmacz, S. Lovas, Development of second generation peptides modulating cellular adiponectin receptor responses, Front Chem. 2 (2014) 93.
[37] L. Bosch, J.J. de Haan, M. Bastemeijer, J. van der Burg, E. van der Worp, M. Wesseling, M. Viola, C. Odille, H. El Azzouzi, G. Pasterkamp, J.P.G. Sluijter, K. E. Wever, S.C.A. de Jager, The transverse aortic constriction heart failure animal model: a systematic review and meta-analysis, Heart Fail Rev. 26 (6) (2021) 1515–1524.
[38] E.E. Creemers, Y.M. Pinto, Molecular mechanisms that control interstitial fibrosis in the pressure-overloaded heart, Cardiovasc Res 89 (2) (2011) 265–272.
[39] M. Mohan, A. Dihoum, I.R. Mordi, A.M. Choy, G. Rena, C.C. Lang, Left Ventricular Hypertrophy in Diabetic Cardiomyopathy: A Target for Intervention, Front Cardiovasc Med 8 (2021) 746382.
[40] M.T. Bourdillon, R.S. Vasan, A Contemporary Approach to Hypertensive Cardiomyopathy: Reversing Left Ventricular Hypertrophy, Curr. Hypertens. Rep. 22 (10) (2020) 85.
[41] X. Han, Y. Wang, M. Fu, Y. Song, J. Wang, X. Cui, Y. Fan, J. Cao, J. Luo, A. Sun, Y. Zou, K. Hu, J. Zhou, J. Ge, Effects of Adiponectin on Diastolic Function in Mice Underwent Transverse Aorta Constriction, J. Cardiovasc Transl. Res 13 (2) (2020) 225–237.
[42] M. Shimano, N. Ouchi, R. Shibata, K. Ohashi, D.R. Pimentel, T. Murohara, K. Walsh, Adiponectin deficiency exacerbates cardiac dysfunction following pressure overload through disruption of an AMPK-dependent angiogenic response, J. Mol. Cell Cardiol. 49 (2) (2010) 210–220.
[43] F. Sam, T.A. Duhaney, K. Sato, R.M. Wilson, K. Ohashi, S. Sono-Romanelli, A. Higuchi, D.S. De Silva, F. Qin, K. Walsh, N. Ouchi, Adiponectin deficiency, diastolic dysfunction, and diastolic heart failure, Endocrinology 151 (1) (2010) 322–331.
[44] R. Shibata, N. Ouchi, M. Ito, S. Kihara, I. Shiojima, D.R. Pimentel, M. Kumada, K. Sato, S. Schiekofer, K. Ohashi, T. Funahashi, W.S. Colucci, K. Walsh, Adiponectin-mediated modulation of hypertrophic signals in the heart, Nat. Med 10 (12) (2004) 1384–1389.
[45] T. Arimura, A. Muchir, M. Kuwahara, S. Morimoto, T. Ishikawa, C.K. Du, D. Y. Zhan, S. Nakao, N. Machida, R. Tanaka, Y. Yamane, T. Hayashi, A. Kimura, Overexpression of heart-specific small subunit of myosin light chain phosphatase results in heart failure and conduction disturbance, Am. J. Physiol. Heart Circ. Physiol. 314 (6) (2018) H1192–H1202.
[46] L. Zhou, F. Peng, J. Li, H. Gong, Exploring novel biomarkers in dilated cardiomyopathy-induced heart failure by integrated analysis and in vitro experiments, Exp. Ther. Med 26 (1) (2023) 325.
[47] S.M. Day, J.C. Tardiff, E.M. Ostap, Myosin modulators: emerging approaches for the treatment of cardiomyopathies and heart failure, J. Clin. Invest 132 (5) (2022).
[48] R.S. Nagalingam, S. Chattopadhyaya, D.S. Al-Hattab, D.Y.C. Cheung, L. Y. Schwartz, S. Jana, N. Aroutiounova, D.A. Ledingham, T.L. Moffatt, N.M. Landry, R.A. Bagchi, I.M.C. Dixon, J.T. Wigle, G.Y. Oudit, Z. Kassiri, D.S. Jassal, M. P. Czubryt, Scleraxis and fibrosis in the pressure-overloaded heart, Eur. Heart J. 43 (45) (2022) 4739–4750.
[49] S. Chattopadhyaya, R.S. Nagalingam, D.A. Ledingham, T.L. Moffatt, D.S. Al-Hattab, P. Narhan, M.T. Stecy, K.A. O'Hara, M.P. Czubryt, Regulation of Cardiac Fibroblast GLS1 Expression by Scleraxis, Cells 11 (9) (2022).
[50] A. Zhu, H. Bews, D. Cheung, R.S. Nagalingam, I. Mittal, V. Goyal, C.Y. Asselin, I.D. C. Kirkpatrick, M.P. Czubryt, D.S. Jassal, Scleraxis as a prognostic marker of myocardial fibrosis in hypertrophic cardiomyopathy (SPARC) study, Can. J. Physiol. Pharm. 98 (7) (2020) 459–465.
[51] C. Koentges, M.E. Pepin, C. Musse, K. Pfeil, S.V.V. Alvarez, N. Hoppe, M. M. Hoffmann, K.E. Odening, S. Sossalla, A. Zirlik, L. Hein, C. Bode, A.R. Wende, H. Bugger, Gene expression analysis to identify mechanisms underlying heart failure susceptibility in mice and humans, Basic Res Cardiol. 113 (1) (2018) 8.
[52] I. Russo, M. Cavalera, S. Huang, Y. Su, A. Hanna, B. Chen, A.V. Shinde, S. J. Conway, J. Graff, N.G. Frangogiannis, Protective Effects of Activated Myofibroblasts in the Pressure-Overloaded Myocardium Are Mediated Through Smad-Dependent Activation of a Matrix-Preserving Program, Circ. Res 124 (8) (2019) 1214–1227.
[53] Q.J. Zhang, T.A.T. Tran, M. Wang, M.J. Ranek, K.M. Kokkonen-Simon, J. Gao, X. Luo, W. Tan, V. Kyrychenko, L. Liao, J. Xu, J.A. Hill, E.N. Olson, D.A. Kass, E. D. Martinez, Z.P. Liu, Histone lysine dimethyl-demethylase KDM3A controls pathological cardiac hypertrophy and fibrosis, Nat. Commun. 9 (1) (2018) 5230.
[54] E.Y. Wang, J. Smith, M. Radisic, Design and Fabrication of Biological Wires for Cardiac Fibrosis Disease Modeling, Methods Mol. Biol. 2485 (2022) 175–190.
[55] E.Y. Wang, N. Rafatian, Y. Zhao, A. Lee, B.F.L. Lai, R.X. Lu, D. Jekic, L. Davenport Huyer, E.J. Knee-Walden, S. Bhattacharya, P.H. Backx, M. Radisic, Biowire Model of Interstitial and Focal Cardiac Fibrosis, ACS Cent. Sci. 5 (7) (2019) 1146–1158.
[56] E.Y. Wang, U. Kuzmanov, J.B. Smith, W. Dou, N. Rafatian, B.F.L. Lai, R.X.Z. Lu, Q. Wu, J. Yazbeck, X.O. Zhang, Y. Sun, A. Gramolini, M. Radisic, An organ-on-a-chip model for pre-clinical drug evaluation in progressive non-genetic cardiomyopathy, J. Mol. Cell Cardiol. 160 (2021) 97–110.
[57] W.J. Paulus, M.R. Zile, From Systemic Inflammation to Myocardial Fibrosis: The Heart Failure With Preserved Ejection Fraction Paradigm Revisited, Circ. Res 128 (10) (2021) 1451–1467.
[58] L. Bacmeister, M. Schwarzl, S. Warnke, B. Stoffers, S. Blankenberg, D. Westermann, D. Lindner, Inflammation and fibrosis in murine models of heart failure, Basic Res Cardiol. 114 (3) (2019) 19.
[59] K. Ohashi, N. Ouchi, Y. Matsuzawa, Anti-inflammatory and anti-atherogenic properties of adiponectin, Biochimie 94 (10) (2012) 2137–2142.
[60] O.A. Segiet, A. Piecuch, L. Mielanczyk, M. Michalski, E. Nowalany-Kozielska, Role of interleukins in heart failure with reduced ejection fraction, Anatol. J. Cardiol. 22 (6 (2019) 287–299.
[61] Y. Nishimura, T. Inoue, T. Nitto, T. Morooka, K. Node, Increased interleukin-13 levels in patients with chronic heart failure, Int J. Cardiol. 131 (3) (2009) 421–423.
[62] N.A. Diakos, I. Taleb, C.P. Kyriakopoulos, K.S. Shah, H. Javan, T.J. Richins, M. Y. Yin, C.G. Yen, E. Dranow, M.J. Bonios, R. Alharethi, A.G. Koliopoulou, M. Taleb, J.C. Fang, C.H. Selzman, K. Stellos, S.G. Drakos, Circulating and Myocardial Cytokines Predict Cardiac Structural and Functional Improvement in Patients With Heart Failure Undergoing Mechanical Circulatory Support, J. Am. Heart Assoc. 10 (20) (2021) e020238.
[63] T.B. Opstad, H. Arnesen, A.A. Pettersen, I. Seljeflot, Combined Elevated Levels of the Proinflammatory Cytokines IL-18 and IL-12 Are Associated with Clinical Events in Patients with Coronary Artery Disease: An Observational Study, Metab. Syndr. Relat. Disord. 14 (5) (2016) 242–248.
[64] U. Bhattarai, X. He, R. Xu, X. Liu, L. Pan, Y. Sun, J.X. Chen, Y. Chen, IL-12alpha deficiency attenuates pressure overload-induced cardiac inflammation, hypertrophy, dysfunction, and heart failure progression, Front Immunol. 14 (2023) 1105664.
[65] X. Kan, Y. Wu, Y. Ma, C. Zhang, P. Li, L. Wu, S. Zhang, Y. Li, J. Du, Deficiency of IL-12p35 improves cardiac repair after myocardial infarction by promoting angiogenesis, Cardiovasc Res 109 (2) (2016) 249–259.
[66] C. Hage, E. Michaelsson, C. Linde, E. Donal, J.C. Daubert, L.M. Gan, L.H. Lund, Inflammatory Biomarkers Predict Heart Failure Severity and Prognosis in Patients With Heart Failure With Preserved Ejection Fraction: A Holistic Proteomic Approach, Circ. Cardiovasc Genet 10 (1) (2017).
[67] A. Safa, H.R. Rashidinejad, M. Khalili, S. Dabiri, M. Nemati, M.M. Mohammadi, A. Jafarzadeh, Higher circulating levels of chemokines CXCL10, CCL20 and CCL22 in patients with ischemic heart disease, Cytokine 83 (2016) 147–157.
[68] C.M. Yang, C.C. Yang, W.H. Hsu, L.D. Hsiao, H.C. Tseng, Y.F. Shih, Tumor Necrosis Factor-alpha-Induced C-C Motif Chemokine Ligand 20 Expression through TNF Receptor 1-Dependent Activation of EGFR/p38 MAPK and JNK1/2/FoxO1 or the NF-kappaB Pathway in Human Cardiac Fibroblasts, Int J. Mol. Sci. 23 (16) (2022).
[69] A. Hanna, N.G. Frangogiannis, Inflammatory Cytokines and Chemokines as Therapeutic Targets in Heart Failure, Cardiovasc Drugs Ther. 34 (6) (2020) 849–863.

[70] C.M. Birner, C. Ulucan, S. Fredersdorf, M. Rihm, H. Lowel, J. Stritzke, H. Schunkert, C. Hengstenberg, S. Holmer, G. Riegger, A. Luchner, Head-to-head comparison of BNP and IL-6 as markers of clinical and experimental heart failure: Superiority of BNP, Cytokine 40 (2) (2007) 89–97.
[71] S. Huo, W. Shi, H. Ma, D. Yan, P. Luo, J. Guo, C. Li, J. Lin, C. Zhang, S. Li, J. Lv, L. Lin, Alleviation of Inflammation and Oxidative Stress in Pressure Overload-Induced Cardiac Remodeling and Heart Failure via IL-6/STAT3 Inhibition by Raloxifene, Oxid. Med Cell Longev. 2021 (2021) 6699054.
[72] J. Wu, E. Dong, Y. Zhang, H. Xiao, The Role of the Inflammasome in Heart Failure, Front Physiol. 12 (2021) 709703.
[73] B.M. Everett, J.G. MacFadyen, T. Thuren, P. Libby, R.J. Glynn, P.M. Ridker, Inhibition of Interleukin-1beta and Reduction in Atherothrombotic Cardiovascular Events in the CANTOS Trial, J. Am. Coll. Cardiol. 76 (14) (2020) 1660–1670.
[74] S. Li, P. Yang, Relationship between HSPA1A-regulated gene expression and alternative splicing in mouse cardiomyocytes and cardiac hypertrophy, J. Thorac. Dis. 13 (9) (2021) 5517–5533.
[75] A. Masuch, M. Pietzner, M. Bahls, K. Budde, G. Kastenmuller, S. Zylla, A. Artati, J. Adamski, H. Volzke, M. Dorr, S.B. Felix, M. Nauck, N. Friedrich, Metabolomic profiling implicates adiponectin as mediator of a favorable lipoprotein profile associated with NT-proBNP, Cardiovasc Diabetol. 17 (1) (2018) 120.
[76] R. Palanivel, R. Ganguly, S. Turdi, A. Xu, G. Sweeney, Adiponectin stimulates Rho-mediated actin cytoskeleton remodeling and glucose uptake via APPL1 in primary cardiomyocytes, Metabolism 63 (10) (2014) 1363–1373.
[77] J. Du, L. Shen, Z. Tan, P. Zhang, X. Zhao, Y. Xu, M. Gan, Q. Yang, J. Ma, A. Jiang, G. Tang, Y. Jiang, L. Jin, M. Li, L. Bai, X. Li, J. Wang, S. Zhang, L. Zhu, Betaine Supplementation Enhances Lipid Metabolism and Improves Insulin Resistance in Mice Fed a High-Fat Diet, Nutrients 10 (2) (2018).
[78] T. Luo, Z. Guo, D. Liu, Z. Guo, Q. Wu, Q. Li, R. Lin, P. Chen, C. Ou, M. Chen, Deficiency of PSRC1 accelerates atherosclerosis by increasing TMAO production via manipulating gut microbiota and flavin monooxygenase 3, Gut Microbes 14 (1) (2022) 2077602.
[79] A. Yurdagul Jr, N. Kong, B.D. Gerlach, X. Wang, P. Ampomah, G. Kuriakose, W. Tao, J. Shi, I. Tabas, ODC (Ornithine Decarboxylase)-Dependent Putrescine Synthesis Maintains MerTK (MER Tyrosine-Protein Kinase) Expression to Drive Resolution, Arterioscler. Thromb. Vasc. Biol. 41 (3) (2021) e144-e159.
[80] T. Eisenberg, M. Abdellatif, S. Schroeder, U. Primessnig, S. Stekovic, T. Pendl, A. Harger, J. Schipke, A. Zimmermann, A. Schmidt, M. Tong, C. Ruckenstuhl, C. Dammbrueck, A.S. Gross, V. Herbst, C. Magnes, G. Trausinger, S. Narath, A. Meinitzer, Z. Hu, A. Kirsch, K. Eller, D. Carmona-Gutierrez, S. Buttner, F. Pietrocola, O. Knittelfelder, E. Schrepfer, P. Rockenfeller, C. Simonini, A. Rahn, M. Horsch, K. Moreth, J. Beckers, H. Fuchs, V. Gailus-Durner, F. Neff, D. Janik, B. Rathkolb, J. Rozman, M.H. de Angelis, T. Moustafa, G. Haemmerle, M. Mayr, P. Willeit, M. von Frieling-Salewsky, B. Pieske, L. Scorrano, T. Pieber, R. Pechlaner, J. Willeit, S.J. Sigrist, W.A. Linke, C. Muhlfeld, J. Sadoshima, J. Dengjel, S. Kiechl, G. Kroemer, S. Sedej, F. Madeo, Cardioprotection and lifespan extension by the natural polyamine spermidine, Nat. Med 22 (12) (2016) 1428–1438.
[81] L. Otvos Jr, E. Haspinger, F. La Russa, F. Maspero, P. Graziano, I. Kovalszky, S. Lovas, K. Nama, R. Hoffmann, D. Knappe, M. Cassone, J. Wade, E. Surmacz, Design and development of a peptide-based adiponectin receptor agonist for cancer treatment, BMC Biotechnol. 11 (2011) 90.